INTERNATIONAL CENTER FOR NUMERICAL METHODS IN ENGINEERING

Numerical Aerodynamic Analysis of Large Buildings Using a Finite Element Model with Application To a Telescope Building

R. Codina
C. Morton
E. Oñate
O. Soto

Publication CIMNE Nº-181, December 1999

Numerical aerodynamic analysis of large buildings using a finite element model with application to a telescope building

Ramon Codina, Christopher Morton, Eugenio Oñate and Orlando Soto

International Center for Numerical Methods in Engineering,
Universitat Politècnica de Catalunya,
Jordi Girona 1-3, Edifici C1, 08034 Barcelona, Spain

Abstract

This paper presents a numerical strategy for the aerodynamic analysis of large buildings, with an application to the simulation of the air flow within in a telescope building. The finite element formulation is presented first, and then the methodology followed to obtain significant data from the calculations is described. The quality of the ventilation of the building is defined by the average residence times, and the feasibility of this ventilation by the actions created on the instruments and the general flow pattern.

Contents

1 Introduction

This paper describes a finite element methodology to analyze the air flow through large buildings, with an application to the prediction of the external and internal aerodynamic behavior of a large telescope facility to be built in La Palma island (Canary Islands, Spain). From the point of view of the design of the telescope, the main objectives are to obtain a qualitative assessment about the air flow within the building, which could give an idea of the quality of the ventilation, and to obtain the actions exerted by the wind on the instruments within the telescope, since it is of fundamental importance to control their vibrations to ensure the quality of the astronomical observations. Of relatively lower importance is the thermal analysis, which can predict temperature fluctuations near the observation instruments responsible for a deterioration of the quality of the visibility.

We describe in this article a strategy to measure the quality of the ventilation through the definition of the average renovation times. The actions exerted by the wind on the instruments are simply given by the evolution in time of the force and the torque on them. The final outcome of the numerical analysis is the temperature distribution within the building.

Referring to the mathematical and numerical models employed, the flow is modeled by the incompressible Navier-Stokes equations using Smagorinsky's turbulence model, and assuming a Boussinesq coupling between the momentum and the heat equations. These equations are discretized in time using the standard trapezoidal rule and in space using a stabilized finite element formulation, which allows in particular to interpolate all the unknowns using linear tetrahedral elements. This stabilized formulation is based on the algebraic version of subgrid scale concept introduced in [1] and is developed in [2, 3]. Similar formulations applied to large scale problems can be found for example in [4, 5]. Finally, the treatment of the turbulence and the thermal coupling is also discussed.

The aerodynamic analysis of the large telescope building is then detailed. The external flow study is discussed first and the different wind analyses to define the precise location taking into account a large amount of land around the telescope building are also described. The final part of the paper presents the ventilation study performed. Here, the study of the air flow through 164 windows and within the telescope building, incorporating all the telescope equipment, is described. The evolution of forces on the main structures are computed in order to know the action of the wind on them. The tracking of the air particles within the building is used to determine average renovation times.

The results presented here are part of a work done in the context of a contract between the International Center for Numerical Methods in Engineering (CIMNE) and GRANTECAN, the Spanish public company in charge of the studies prior to the construction of the telescope.

2 Numerical model

2.1 Problem statement

In this section we shall consider the flow problem for an incompressible fluid taking into account the coupling of the Navier-Stokes equations with the heat transport equation through Boussinesq's assumption, as well as a nonlinear viscosity dependence on the velocity gradient invariants through Smagorinsky's turbulence model.

The equations describing the problem are

$$\partial_t \boldsymbol{u} + (\boldsymbol{u}\cdot\nabla)\boldsymbol{u} - 2\nabla\cdot[\nu\boldsymbol{\varepsilon}(\boldsymbol{u})] + \nabla p + \beta\boldsymbol{g}\vartheta = \boldsymbol{f}, \tag{1}$$

$$\nabla\cdot\boldsymbol{u} = 0, \tag{2}$$

$$\partial_t\vartheta + (\boldsymbol{u}\cdot\nabla)\vartheta - \nabla\cdot(\kappa\nabla\vartheta) = 0, \tag{3}$$

to be solved in $\Omega\times(0,t_{\text{fin}})$, where $\Omega\subset\mathbb{R}^3$ is the computational domain and $[0,t_{\text{fin}}]$ is the time interval to be considered. In (1)-(3), $\boldsymbol{u}$ denotes the velocity field, p is the kinematic pressure (i.e., the pressure divided by the density), ϑ is the temperature, ν is the total kinematic viscosity (physical plus turbulent), $\boldsymbol{\varepsilon}(\boldsymbol{u})$ is the symmetrical part of the velocity gradient, β is the thermal expansion coefficient, $\boldsymbol{g}$ is the gravity acceleration vector, $\boldsymbol{f}$ is the vector of body forces, and κ is the thermal diffusivity (that is, the thermal conductivity divided by the heat capacity). The density ρ_0 is assumed constant to obtain equations (1)-(3). In the numerical examples, all these properties have been taken as those corresponding to air in normal conditions.

The force vector $\boldsymbol{f}$ in (1) contains the reference buoyancy forces from Boussinesq's assumption, that is

$$\boldsymbol{f} = \boldsymbol{g}(1+\beta\vartheta_0).$$

In this equation, ϑ_0 is the reference temperature from which buoyancy forces are computed.

Smagorinsky's turbulence model has been employed in the numerical simulations. This model is tight to the numerical discretization in space of the flow equations, which in our case is performed using the finite element method. The turbulent kinematic viscosity associated to this model is

$$\nu_t = \rho_0^{-1} c h^2 \left[\boldsymbol{\varepsilon}(\boldsymbol{u}) : \boldsymbol{\varepsilon}(\boldsymbol{u})\right]^{1/2},$$

where c is a constant, usually taken as $c = 0.01$, the colon stands for the double contraction of second order tensors and h is the length of the element where the turbulent kinematic viscosity is to be computed.

In order to write the boundary conditions for equations (1)-(3), consider the boundary $\Gamma = \partial\Omega$ split into sets of disjoint components as $\Gamma = \overline{\Gamma_{\text{dv}}\cup\Gamma_{\text{nv}}\cup\Gamma_{\text{mv}}}$ and also as $\Gamma = \overline{\Gamma_{\text{dt}}\cup\Gamma_{\text{nt}}}$, where Γ_{dv} and Γ_{dt} are the parts of the boundary with Dirichlet type boundary conditions for

the velocity and the temperature, respectively, and $\Gamma_{\rm nv}$ and $\Gamma_{\rm nt}$ are those where Neumann type conditions are prescribed. Mixed boundary conditions for the velocity are fixed on $\Gamma_{\rm mv}$. If the Cauchy stress tensor (divided by the density) is written as $\boldsymbol{\sigma} = -p\boldsymbol{I} + 2\nu\boldsymbol{\varepsilon}(\boldsymbol{u})$, the exterior normal to $\partial\Omega$ is $\boldsymbol{n}$, and prescribed values are represented by an overbar, the boundary conditions to be considered are

$$\boldsymbol{u}(\boldsymbol{x},t) = \bar{\boldsymbol{u}}(\boldsymbol{x},t) \quad \text{on} \quad \Gamma_{\rm dv}, \tag{4}$$

$$\boldsymbol{n}\cdot\boldsymbol{\sigma}(\boldsymbol{x},t) = \boldsymbol{0} \quad \text{on} \quad \Gamma_{\rm nv}, \tag{5}$$

$$\boldsymbol{n}\cdot\boldsymbol{u}(\boldsymbol{x},t) = 0 \ \text{ and } \ \boldsymbol{n}\cdot\boldsymbol{\sigma}(\boldsymbol{x},t)|_{\rm tang} = \bar{\boldsymbol{t}} \quad \text{on} \quad \Gamma_{\rm mv}, \tag{6}$$

$$\vartheta(\boldsymbol{x},t) = \bar{\vartheta}(\boldsymbol{x},t) \quad \text{on} \quad \Gamma_{\rm dt}, \tag{7}$$

$$\kappa\,\boldsymbol{n}\cdot\nabla\vartheta(\boldsymbol{x},t) = 0 \quad \text{on} \quad \Gamma_{\rm nt}, \tag{8}$$

for $t \in (0, t_{\rm fin})$. In (6), $\boldsymbol{n}\cdot\boldsymbol{\sigma}(\boldsymbol{x},t)|_{\rm tang}$ denotes the component of the stress vector $\boldsymbol{n}\cdot\boldsymbol{\sigma}(\boldsymbol{x},t)$ tangent to $\partial\Omega$ and $\bar{\boldsymbol{t}}$ is the stress resulting from the standard wall law

$$\bar{\boldsymbol{t}} = -\rho_0 \frac{U_*^2}{|\boldsymbol{u}|}\boldsymbol{u},$$

where U_* is the solution of the nonlinear equation

$$\frac{|\boldsymbol{u}|}{U_*} = \frac{1}{\kappa}\log\left(\frac{U_*\Delta}{\nu}\right) + C,$$

with $\kappa = 0.41$ (von Kármán constant), $C = 5.5$ and where Δ is the distance from the wall at which the velocity is evaluated.

To close the problem, initial conditions have to be appended to equations (1)-(3) and the boundary conditions (4)-(8). They are of the form $\boldsymbol{u}(\boldsymbol{x},0) = \boldsymbol{u}^0(\boldsymbol{x})$, $\vartheta(\boldsymbol{x},0) = \vartheta^0(\boldsymbol{x})$ for $\boldsymbol{x} \in \Omega$, where $\boldsymbol{u}^0(\boldsymbol{x})$ is a given initial velocity and $\vartheta^0(\boldsymbol{x})$ a given initial temperature.

In the numerical simulations of the telescope building, $\Gamma_{\rm dv}$ corresponds to the inflow part of the boundary of the computational domain, where the wind velocity is prescribed to a certain value of interest and with a given direction, whereas $\Gamma_{\rm nv}$ is the outflow boundary. The surface $\Gamma_{\rm mv}$ corresponds to both the ground surface and the building surface.

2.2 Time discretization

Let us consider now the temporal discretization of equations (1)-(3), for which we use the generalized trapezoidal rule. Let $0 = t^0 < t^1 < ... < t^N = t_{\rm fin}$ be a partition of the time interval and $\alpha \in [0,1]$. To simplify the notation, we shall take the time step size $\delta t := t^{n+1} - t^n$ constant for all n. Let us also introduce the notation

$$\delta f^n := f^{n+1} - f^n,$$
$$f^{n+\alpha} := \alpha f^{n+1} + (1-\alpha) f^n,$$
$$\delta_t f^n := \frac{\delta f^n}{\delta t},$$

where f is a generic function of time and f^n denotes the value of f at time t^n or an approximation to it.

Assuming all the functions involved continuous in time, the trapezoidal rule applied to equations (1)-(3) leads to the following time discrete problem: from known $\boldsymbol{u}^n$ and ϑ^n, find $\boldsymbol{u}^{n+1}$, p^{n+1} and ϑ^{n+1} such that

$$\delta_t \boldsymbol{u}^n + (\boldsymbol{u}^{n+\alpha} \cdot \nabla)\boldsymbol{u}^{n+\alpha} - 2\nabla \cdot [\nu^{n+\alpha}\boldsymbol{\varepsilon}(\boldsymbol{u}^{n+\alpha})] + \nabla p^{n+1} + \boldsymbol{g}\beta\vartheta^{n+\alpha} = \boldsymbol{f}^{n+\alpha}, \tag{9}$$

$$\nabla \cdot \boldsymbol{u}^{n+1} = 0, \tag{10}$$

$$\delta_t \vartheta^n + (\boldsymbol{u}^{n+\alpha} \cdot \nabla)\vartheta^{n+\alpha} - \nabla \cdot (\kappa \nabla \vartheta^{n+\alpha}) = 0, \tag{11}$$

and satisfying the boundary conditions described before. Observe that the problem can be posed in terms of $\boldsymbol{u}^{n+\alpha}$ and $\vartheta^{n+\alpha}$ rather than $\boldsymbol{u}^{n+1}$ and ϑ^{n+1} by using the fact that $\delta f^n = (f^{n+\alpha} - f^n)/\alpha$, for any function f.

The values of interest of the parameter α are $\alpha = 1/2$ and $\alpha = 1$, corresponding to the Crank-Nicholson and the backward Euler schemes, respectively. Both are unconditionally stable, although the former is expected to be second order accurate whereas only a first order approximation can be expected for the latter.

2.3 Finite element approximation

Once the time discretization has been carried out, we are left with the boundary value problem defined by the differential equations (9)-(11). In order to discretize it in space, let $\{\Omega^e\}$ be a finite element partition of the domain Ω, with index e ranging from 1 to the number of elements n_{el}. We denote with a subscript h the finite element approximation to the unknown functions, and by $\boldsymbol{v}_h$, q_h and ψ_h the velocity, pressure and temperature test functions associated to $\{\Omega^e\}$, respectively.

A very important point is that we are interested in *using equal interpolation for all the unknowns* (velocity, pressure and temperature). Therefore, all the finite element spaces are assumed to be built up using the standard continuous interpolation functions. In particular, all the numerical simulations have been carried out using meshes of linear tetrahedra.

In order to overcome the numerical problems of the standard Galerkin method, a stabilized finite element formulation is applied. This formulation is presented in [2] for the general case of systems of convection-diffusion-reaction equations, and applied to the Navier-Stokes equations in [3], where its convergence properties for the linearized problem are analyzed. It is based on the subgrid scale concept introduced in [1], although when linear elements are used it reduces to the Galerkin/least-squares method described for example in [6, 7, 4]. As in [6], we apply this stabilized formulation together with the finite difference approximation in time described above. The bottom line of the method is to test the continuous equations by the standard Galerkin test functions plus perturbations that depend on the operator representing the differential equation being solved. In our case, this operator corresponds to the linearized

form of the time-discrete Navier-Stokes equations (9)-(10) and the heat equation (11). In this case, the method consists of finding $\boldsymbol{u}_h^{n+\alpha}$, p_h^{n+1} and $\vartheta_h^{n+\alpha}$ such that

$$\begin{aligned}
&\int_\Omega \boldsymbol{v}_h \cdot \boldsymbol{r}_{u1}^{n+\alpha}\,\mathrm{d}\Omega + \int_\Omega 2\boldsymbol{\varepsilon}(\boldsymbol{v}_h) : \nu^{n+\alpha}\boldsymbol{\varepsilon}(\boldsymbol{u}_h^{n+\alpha})\,\mathrm{d}\Omega - \int_\Omega p_h^{n+1}\nabla\cdot\boldsymbol{v}_h\,\mathrm{d}\Omega \\
&\quad + \sum_{e=1}^{n_{\mathrm{el}}} \int_{\Omega^e} \boldsymbol{\zeta}_{u1}^{n+\alpha}\cdot\left(\boldsymbol{r}_{u1}^{n+\alpha}+\boldsymbol{r}_{u2}^{n+\alpha}\right)\,\mathrm{d}\Omega + \sum_{e=1}^{n_{\mathrm{el}}} \int_{\Omega^e} \zeta_{u2}^{n+\alpha}\, r_p^{n+\alpha}\,\mathrm{d}\Omega \\
&\quad = \sum_{e=1}^{n_{\mathrm{el}}} \int_{\Omega^e} \left(\boldsymbol{v}_h + \boldsymbol{\zeta}_{u1}^{n+\alpha}\right)\cdot\boldsymbol{f}^{n+\alpha}\,\mathrm{d}\Omega + \int_{\Gamma_{\mathrm{mv}}} \boldsymbol{v}_h\cdot\bar{\boldsymbol{t}}^{n+\alpha}\,\mathrm{d}\Gamma, \\
&\int_\Omega q_h r_p^{n+\alpha}\,\mathrm{d}\Omega + \sum_{e=1}^{n_{\mathrm{el}}} \int_{\Omega^e} \boldsymbol{\zeta}_p^{n+\alpha}\cdot\left(\boldsymbol{r}_{u1}^{n+\alpha}+\boldsymbol{r}_{u2}^{n+\alpha}\right)\,\mathrm{d}\Omega = \sum_{e=1}^{n_{\mathrm{el}}} \int_{\Omega^e} \boldsymbol{\zeta}_p^{n+\alpha}\cdot\boldsymbol{f}^{n+\alpha}\,\mathrm{d}\Omega, \\
&\int_\Omega \psi_h\cdot r_{\vartheta 1}^{n+\alpha}\,\mathrm{d}\Omega + \int_\Omega \kappa\nabla\psi_h\cdot\nabla\vartheta_h^{n+\alpha}\,\mathrm{d}\Omega + \sum_{e=1}^{n_{\mathrm{el}}} \int_{\Omega^e} \zeta_\vartheta^{n+\alpha}\left(r_{\vartheta 1}^{n+\alpha}+r_{\vartheta 2}^{n+\alpha}\right)\,\mathrm{d}\Omega = 0,
\end{aligned}$$

for all test functions $\boldsymbol{v}_h$, q_h and ψ_h, where

$$\boldsymbol{r}_{u1}^{n+\alpha} := \delta_t \boldsymbol{u}_h^n + \boldsymbol{g}\beta\vartheta_h^{n+\alpha} + (\boldsymbol{u}_h^{n+\alpha}\cdot\nabla)\boldsymbol{u}_h^{n+\alpha}, \tag{12}$$

$$\boldsymbol{r}_{u2}^{n+\alpha} := -2\nabla\cdot[\nu^{n+\alpha}\boldsymbol{\varepsilon}(\boldsymbol{u}_h^{n+\alpha})] + \nabla p_h^{n+1}, \tag{13}$$

$$r_p^{n+\alpha} := \nabla\cdot\boldsymbol{u}_h^{n+\alpha}, \tag{14}$$

$$r_{\vartheta 1}^{n+\alpha} := \delta_t\vartheta_h^n + (\boldsymbol{u}_h^{n+\alpha}\cdot\nabla)\vartheta_h^{n+\alpha}, \tag{15}$$

$$r_{\vartheta 2}^{n+\alpha} := -\nabla\cdot\left(\kappa\cdot\nabla\vartheta_h^{n+\alpha}\right), \tag{16}$$

the functions $\boldsymbol{\zeta}_{u1}$, ζ_{u2} and $\boldsymbol{\zeta}_p$ are computed within each element as

$$\boldsymbol{\zeta}_{u1} = \tau_u\left\{(\boldsymbol{u}_h\cdot\nabla)\boldsymbol{v}_h + 2\nabla\cdot[\nu\boldsymbol{\varepsilon}(\boldsymbol{v}_h)]\right\}, \tag{17}$$

$$\zeta_{u2} = \tau_p\nabla\cdot\boldsymbol{v}_h, \tag{18}$$

$$\boldsymbol{\zeta}_p = \tau_u\nabla q_h, \tag{19}$$

$$\zeta_\vartheta = \tau_\vartheta\left[(\boldsymbol{u}_h\cdot\nabla)\psi_h + \nabla\cdot(\kappa\nabla\psi_h)\right], \tag{20}$$

and the parameters τ_u, τ_p and τ_ϑ are also computed element-wise as (see [8, 3])

$$\begin{aligned}
\tau_u &= \left[\frac{4\nu}{h^2} + \frac{2|\boldsymbol{u}_h|}{h}\right]^{-1}, \\
\tau_p &= 4\nu + 2|\boldsymbol{u}_h|h, \\
\tau_\vartheta &= \left[\frac{4\kappa}{h^2} + \frac{2|\boldsymbol{u}_h|}{h}\right]^{-1},
\end{aligned}$$

where h is the element size for linear elements and half of it for quadratics.

There are several remarks to be made to the previous equations:

REMARK 1. It is observed that (13) and (16) (the terms of the original differential equations integrated by parts in the weak form of the problem) involve second derivatives of the

unknowns. This is why the integrals involving these terms have to be evaluated element by element.

REMARK 2. From (17)-(20) it is observed that these terms are precisely the adjoints of the (linearized) operators of the differential equations to be solved applied to the test functions (observe the signs of the viscous term in (17) and of the diffusive term in (20)). This method corresponds to the algebraic version of the subgrid scale approach ([1, 2]) and circumvents *all* the stability problems of the Galerkin method. In particular, in this case it is possible to use equal velocity pressure interpolations, that is, we are not tight to the satisfaction of the inf-sup stability condition. □

2.4 Linearized equations and iterative coupling

The final step is to linearize the previous finite element problem. In our case, there are two sources of nonlinearity, namely, the convective term of the Navier-Stokes and the heat equations and the fact that the viscosity depends in a nonlinear way on the viscosity through the turbulence model. We have used the simplest fixed point scheme to linearize these nonlinearities.

The convective term in the heat equation is another nonlinearity of the problem. However, instead of linearizing this term and dealing with the fully coupled problem, with velocity, pressure and temperature as unknowns, we use an iterative coupling, as described for example in [9]. The idea is to use the temperature known from the previous iteration in the momentum equation, and then use this equation and the continuity equation to compute the velocity and the pressure. With the velocity computed, we can proceed to solve the heat transport equation. Using this strategy, the fully discrete and linearized system of equations to be solved is

$$
\begin{aligned}
&\int_\Omega \boldsymbol{v}_h \cdot \boldsymbol{r}_{u1}^{n+\alpha,i+1}\,\mathrm{d}\Omega + \int_\Omega 2\boldsymbol{\varepsilon}(\boldsymbol{v}_h) : \nu^{n+\alpha,i}\boldsymbol{\varepsilon}(\boldsymbol{u}_h^{n+\alpha,i+1})\,\mathrm{d}\Omega - \int_\Omega p_h^{n+1,i+1}\nabla\cdot\boldsymbol{v}_h\,\mathrm{d}\Omega \\
&\qquad + \sum_{e=1}^{n_{\mathrm{el}}} \int_{\Omega^e} \boldsymbol{\zeta}_{u1}^{n+\alpha,i}\cdot\left(\boldsymbol{r}_{u1}^{n+\alpha,i+1} + \boldsymbol{r}_{u2}^{n+\alpha,i+1}\right)\,\mathrm{d}\Omega + \sum_{e=1}^{n_{\mathrm{el}}} \int_{\Omega^e} \zeta_{u2}^{n+\alpha,i}\, r_p^{n+\alpha,i+1}\,\mathrm{d}\Omega \\
&\qquad = \sum_{e=1}^{n_{\mathrm{el}}} \int_{\Omega^e} \left(\boldsymbol{v}_h + \boldsymbol{\zeta}_{u1}^{n+\alpha,i}\right)\cdot\boldsymbol{f}^{n+\alpha}\,\mathrm{d}\Omega + \int_{\Gamma_{\mathrm{mv}}} \boldsymbol{v}_h\cdot\bar{\boldsymbol{t}}^{n+\alpha}\,\mathrm{d}\Gamma, \\
&\int_\Omega q_h r_p^{n+\alpha,i+1}\,\mathrm{d}\Omega + \sum_{e=1}^{n_{\mathrm{el}}} \int_{\Omega^e} \boldsymbol{\zeta}_p^{n+\alpha,i}\cdot\left(\boldsymbol{r}_{u1}^{n+\alpha,i+1} + \boldsymbol{r}_{u2}^{n+\alpha,i+1}\right)\,\mathrm{d}\Omega \\
&\qquad = \sum_{e=1}^{n_{\mathrm{el}}} \int_{\Omega^e} \boldsymbol{\zeta}_p^{n+\alpha,i}\cdot\boldsymbol{f}^{n+\alpha}\,\mathrm{d}\Omega, \\
&\int_\Omega \psi_h \cdot r_{\vartheta 1}^{n+\alpha,i+1}\,\mathrm{d}\Omega + \int_\Omega \kappa\nabla\psi_h\cdot\nabla\vartheta_h^{n+\alpha,i+1}\,\mathrm{d}\Omega \\
&\qquad + \sum_{e=1}^{n_{\mathrm{el}}} \int_{\Omega^e} \zeta_\vartheta^{n+\alpha,i}\left(r_{\vartheta 1}^{n+\alpha,i+1} + r_{\vartheta 2}^{n+\alpha,i+1}\right)\,\mathrm{d}\Omega = 0,
\end{aligned}
$$

where the second superscript denotes the iteration counter and

$$
\begin{aligned}
\boldsymbol{r}_{u1}^{n+\alpha,i+1} &:= \delta_t \boldsymbol{u}_h^{n,i+1} + \boldsymbol{g}\beta\vartheta_h^{n+\alpha,i} + (\boldsymbol{u}_h^{n+\alpha,i}\cdot\nabla)\boldsymbol{u}_h^{n+\alpha,i+1},\\
\boldsymbol{r}_{u2}^{n+\alpha,i+1} &:= -2\nabla\cdot[\nu^{n+\alpha,i}\boldsymbol{\varepsilon}(\boldsymbol{u}_h^{n+\alpha,i+1})] + \nabla p_h^{n+1,i+1},\\
r_p^{n+\alpha,i+1} &:= \epsilon p_h^{n+1,i+1} - \lambda\epsilon p_h^{n+1,i} + \nabla\cdot\boldsymbol{u}_h^{n+\alpha,i+1},\\
r_{\vartheta 1}^{n+\alpha,i+1} &:= \delta_t\vartheta_h^{n,i+1} + (\boldsymbol{u}_h^{n+\alpha,i+1}\cdot\nabla)\vartheta_h^{n+\alpha,i+1},\\
r_{\vartheta 2}^{n+\alpha,i+1} &:= -\nabla\cdot\left(\kappa\cdot\nabla\vartheta_h^{n+\alpha,i+1}\right),
\end{aligned}
\tag{21}
$$

In (21) we have introduced a parameter ϵ that corresponds to a penalty parameter for the incompressibility constraint. Likewise, we have introduced the parameter λ, whose values of interest are $\lambda = 0$ and $\lambda = 1$. When $\lambda = 0$ the penalty strategy can be considered the 'classical' one. On the other hand, when $\lambda = 1$ it is seen from (21) that the effect of the penalization disappears when convergence is achieved. This *iterative penalty* method is discussed and analyzed in [10]. The benefit of taking $\lambda = 1$ is that larger values of ϵ may be used with a good approximation of the incompressibility constraint. The use of penalty methods when continuous pressures are used, as in our case, may help to improve the convergence of the iterative methods if they are used to solve the algebraic system of equations, which in the aerodynamic analyses to be described in the following section is the GMRES algorithm with a simple diagonal scaling.

In all the numerical simulations described in the following, convergence within each time step has been specified to 0.1% in the relative mean square norm of the velocities. Although case dependent, around three iterations per time step are required to converge when the flow is fully developed.

3 Numerical aerodynamic analysis of large buildings

3.1 External aerodynamic analysis

The first step in the design of a large building is to define its location. The decision regarding this point may be taken with the help of the numerical aerodynamic analysis of the wind in the region of interest, which may give a qualitative flow pattern relevant at the moment of deciding the building location. Likewise, this preliminary analysis can be used to determine the boundary conditions for a more accurate calculation of the air flow surrounding the building. These boundary conditions can be obtained assuming that the flow far from the building is unaffected by it.

In the following we describe the methodology that we have followed in the aerodynamic analysis of the telescope building to be constructed in the Canary Islands. This methodology consists of the following three steps:

1. Analysis of a large region of land where the building can be placed. The boundary conditions for this analysis are rough wind data (in our case, only the wind direction and its magnitude was considered).

2. Analysis of the region surrounding the building location. Boundary conditions are obtained from the previous step. The effect of the building on the flow is still assumed to be negligible.

3. Analysis of the interior of the building and a (relatively small) exterior region surrounding it. Once again, boundary conditions are obtained from the results of the previous step.

Steps 1 and 2 correspond to the external aerodynamic analysis. In our case, their objective was to analyze the effect of the orography on the air circulation in the telescope location, assuming that the perturbation induced by the building on the flow pattern is negligible.

Two computational domains were considered. The first consists of a square of 6×6 km surrounding the location selected for the telescope with an average height of 1600 m. On the inflow sides of this domain, a wind velocity was prescribed with orientations North-East (NE) and North-West (NW). Experimental data revealed that characteristic velocity values in this area are 2, 4, 6 and 10 m/s. In all the analyses it was necessary to consider low velocities as well as high ones, since the former may lead to poor ventilation of the telescope building and the latter to excessive actions (forces and torques) on the instruments.

For this domain, a mesh of 74 999 elements was used for the spatial discretization. This mesh is too coarse to capture all the details of the flow, and in particular a stationary solution was found. Even though localized flow oscillations were not captured, the velocity field obtained was used (after appropriate interpolation) as boundary condition for the analysis on a finer mesh of 91 604 elements in a smaller domain of 1.5×1.5 km and average height of 450 m. This domain is shown in Figure 1.

The flow pattern computed in this domain is not stationary any more. Multiple vortex shedding and flow separation occur, leading to a complex time behavior. Calculations were performed for a time period of 200 s, with a time step size of 4 s. A sample of the results obtained is shown in Figure 2, where the pressure contours at different sections for a NW wind of 10 m/s are shown.

From the design point of view, these calculations serve to decide whether the telescope location is adequate or not. The main result is the qualitative flow pattern, which shows if local wind accelerations or vortexes occur in the telescope location.

3.2 Air regeneration

After having carried out steps 1 and 2 described in the previous subsection, the internal aerodynamic analysis can be performed. This can give different types of relevant information.

As before, we describe here how to obtain some results that can be of interest in the context of the analysis of the telescope building.

Once the exact location was decided, partly based on the external aerodynamic analysis, the next step was to investigate the possibility of using natural ventilation, which was the original motivation to undertake this study. The target was to obtain 16 air renovations per hour. First of all, the concept of *renovation* has to be precisely defined. Since some of the air particles may remain within the building for ever due to the existence of recirculation regions, it does not make sense to define *renovation* affecting all the air particles. Therefore, this concept must be related to a certain percentage of these particles. We say that this percentage has n renovations per hour if all of them stay within the building less than $3600/n$ seconds. In particular, the target of 16 air renovations per hour can be expressed by requiring that most of the air particles (the 95%, say) stay within the telescope building less that 225 seconds. The methodology that we have employed to obtain an estimate for these quantities is described below.

To perform the internal aerodynamic analysis, the domain of analysis chosen is a square of 300 m side surrounding the building and including it. This building has 164 windows that originally were assumed to be completely open. A general view of the computational domain and the telescope is shown in Figures 3, 4, where the sections used to represent numerical results are also indicated.

The finite element mesh employed in the numerical simulations consists of 460 000 tetrahedra (see Figure 5). The time step size chosen was 2 s, which was found to be small enough to capture the main flow oscillations.

A number of different flow situations was considered, obtained by varying the velocity magnitude, changing the orientation of the building dome, considering different window openings, etc. As mentioned in the description of the general strategy, the velocity boundary conditions were taken from the interpolation of the results obtained in the external aerodynamic analysis.

The first series of analysis corresponded to a wind velocity of 4 m/s (in the outer region) with a NE orientation. In this case, the local average velocities turned out to be of 5.2 m/s. The dome orientations analyzed were 0°, 45°, 90° and 180° with respect to the wind direction. As for the wind magnitude, the better the situation for the air regeneration, the higher the actions on the instruments. The dome has an opening for the telescope device that allows different opening angles with respect to the horizontal line. Most calculations were done assuming an opening of 60°.

Figures 6, 7 show an example of flow pattern inside the telescope building (it corresponds to a NE wind of 4 m/s with the dome rotated 45° west-wards).

In all the cases analyzed, the most important result was the average residence time, which was used as indicative of the quality of the ventilation. This was computed as the

time needed for the particles to abandon the telescope building. We took 830 particles, uniformly distributed within the telescope, and computed the time they spent within the building assuming the flow to be stationary, which is a "conservative" assumption since time fluctuations prevent from stationary vortexes that remain in the building for ever. This was done for several time steps in which the flow was completely developed, showing only small differences in the results. An example of the results obtained is shown in Figure 8, where the percentage of particles in a given time interval to leave the building is given (this figure corresponds to the same case as Figures 6, 7).

The worst situation among those analyzed was that corresponding to a NE velocity of 2 m/s, with the dome orientation at 90° and the windows partially closed. However, even in this case the target of 16 air renovations per hour was accomplished, since in all the cases less than 5 % of the air particles stayed within the building more than 180 seconds.

3.3 Thermal analysis

In the particular case of the telescope building that we are considering, one of the factors that may influence the visibility of the telescope is the temperature distribution. This is why a coupled thermal analysis was performed in some of the cases of air regeneration. The physical model used was based on the Boussinesq assumption, so that the equations describing the problem are those of Section 2, approximated using the numerical strategy described there.

As data for the numerical simulation the wind temperature in the far field was assumed to be of 10° C. Likewise, the ground temperature and the temperatures on the instruments were assumed to be known. The values adopted were chosen according to the indications provided by GRANTECAN. The highest temperature prescribed was 15° C.

Figure 9 shows the temperature distribution obtained at a time step in which the flow was completely developed.

The main conclusion drawn from the thermal analysis was that for the type of ventilation considered convection is dominant in the heat transport process. Heat emanating from the instruments is rapidly transported out of the telescope building, whose mean temperature is close to that of the far field wind.

3.4 Loads on the instruments

Another objective of the aerodynamic analysis of the interior of a building can be to obtain the forces and torques that the wind exerts on its components. These can be computed by integrating the stress vector

$$\boldsymbol{t} = \rho_0 \left[-p\boldsymbol{n} + 2\nu \boldsymbol{n} \cdot \boldsymbol{\varepsilon}(\boldsymbol{u}) \right]$$

and its moment $\boldsymbol{r} \times \boldsymbol{t}$ ($\boldsymbol{r}$ being the position vector) over the surface of the body where the force and torque is needed. If the flow is time dependent, so will be these actions. Therefore,

it can be also interesting to obtain their spectrum, which will provide information about the dominating frequencies in the flow.

In the particular case we are analyzing, high ventilation in the telescope building has the potential danger of causing excessive actions on the instruments inside it. If wind velocities are too high, the forces and torques created on the optical instruments may cause unacceptable vibrations, thus deteriorating the quality of the visibility.

Wind loads on several devices within the telescope building were computed. In order to simplify the mesh generation, these instruments were idealized as shown in Figure 10. There, the primary and secondary lenses are represented, as well as the ring structure supporting them and the devices to activate them. The bar frame connecting the lenses is not taken into account in our analysis.

The forces computed were highly oscillatory in time. An example of the results obtained is presented in Figure 11, where the evolution of the total force on the lower mirror is plotted for a certain position of the telescope opening and orientation of the telescope itself.

Due to the high temporal variation of the wind loads, which is a consequence of the multiple frequencies existing in the flow, it was considered convenient to give as result of the calculation the maximum and minimum loads in time. Also, the Fourier transform of the temporal evolution of the loads in time was computed. Even though some dominant frequencies were observed in some cases, that was not the general rule, which again was an indication of the high number of interacting fluctuations in the flow.

4 Conclusions

In this paper we have presented a numerical model to analyze incompressible flow problems, as well as a strategy to apply it to the aerodynamic analysis of large buildings. In particular, the description of this strategy has been supported by an application to a telescope building where the main goal was to study the possibility of using natural ventilation. The basic tool for the numerical simulations is a finite element method which has proved to be very robust and accurate.

The first step of the study was the external aerodynamic analysis in a large domain to obtain appropriate boundary conditions for the analysis in a smaller region, the results of which were in turn used as boundary conditions for the simulation of the air flow around the building and in its interior.

Three different types of results were obtained from the series of simulations performed. The first is the flow pattern, which may give an indication of possible visibility problems (due for example to the dust that the air can carry). The second is the average residence time, as defined in this paper, which can be used to quantify the quality of the ventilation. Finally, the forces and torques on the instruments in the interior of the building need to be known to

prevent possible vibration problems that could also affect the quality of the visibility.

Acknowledgment

This work was carried out with financial support from GRANTECAN S.A. The conversations with C. Mitirello and G. Pescador helped us to set up the numerical strategy described in this paper. The help of A. León in preparing the numerical results is also acknowledged.

References

[1] T.J.R. Hughes. Multiscale phenomena: Green's function, the Dirichlet-to-Neumann formulation, subgrid scale models, bubbles and the origins of stabilized formulations. *Computer Methods in Applied Mechanics and Engineering*, 127:387–401, 1995.

[2] R. Codina. On stabilized finite element methods for linear systems of convection-diffusion-reaction equations. *Computer Methods in Applied Mechanics and Engineering*, submitted.

[3] R. Codina. A stabilized finite element method for generalized stationary incompressible flows. *Computer Methods in Applied Mechanics and Engineering*, submitted.

[4] T.E. Tezduyar, S. Mittal, S.E. Ray, and R. Shih. Incompressible flow computations with stabilized bilinear and linear equal-order-interpolation velocity-pressure elements. *Computer Methods in Applied Mechanics and Engineering*, 95:221–242, 1992.

[5] T. Tezduyar, S. Aliabadi, M. Berh, A. Jonhson, V. Kalro, and M. Litke. Flow simulation and high performance computing. *Computational Mechanics*, 18:397–412, 1996.

[6] L.P. Franca and S.L. Frey. Stabilized finite element methods: II. The incompressible Navier-Stokes equations. *Computer Methods in Applied Mechanics and Engineering*, 99:209–233, 1992.

[7] F. Shakib, T.J.R. Hughes, and Z. Johan. A new finite element method for computational fluid dynamics: X. the compressible euler and navier-stokes equations. *Computer Methods in Applied Mechanics and Engineering*, 89:141–219, 1991.

[8] R. Codina. Comparison of some finite element methods for solving the diffusion-convection-reaction equation. *Computer Methods in Applied Mechanics and Engineering*, 156:185–210, 1998.

[9] M. Cervera, R. Codina, and M. Galindo. On the computational efficiency and implementation of block-iterative algorithms for nonlinear coupled problems. *Engineering Computations*, 13(6):4–30, 1996.

[10] R. Codina. An iterative penalty method for the finite element solution of the stationary Navier-Stokes equations. *Computer Methods in Applied Mechanics and Engineering*, 110:237–262, 1993.

List of Figures

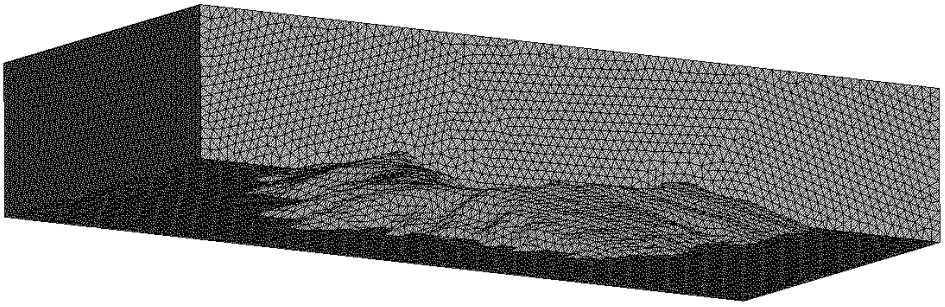

Figure 1: Domain and surface mesh surrounding the telescope location

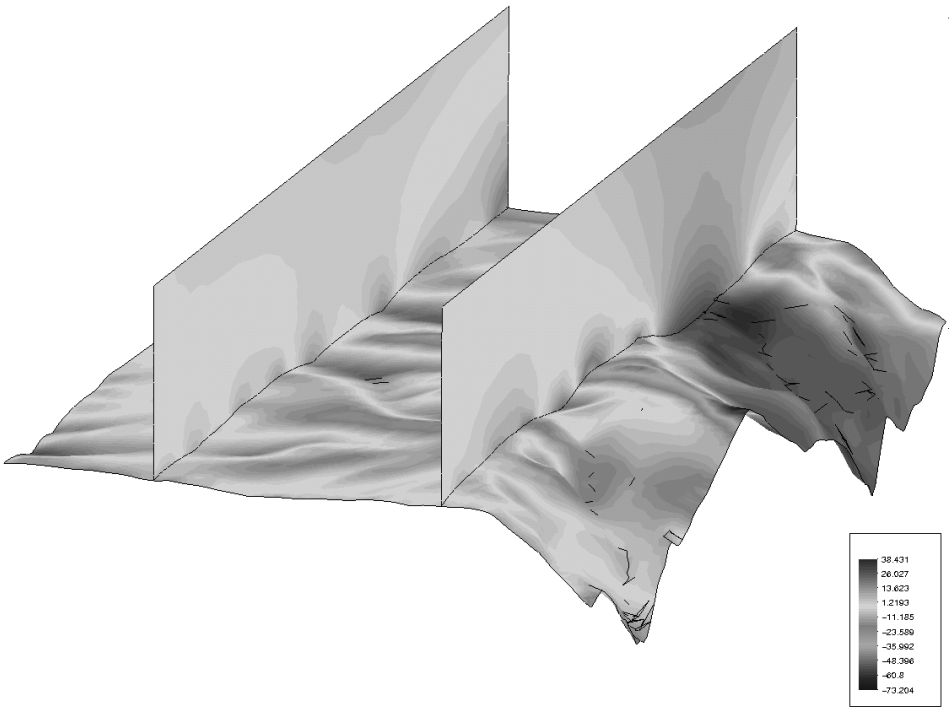

Figure 2: Pressure contours for a NW wind of 10 m/s

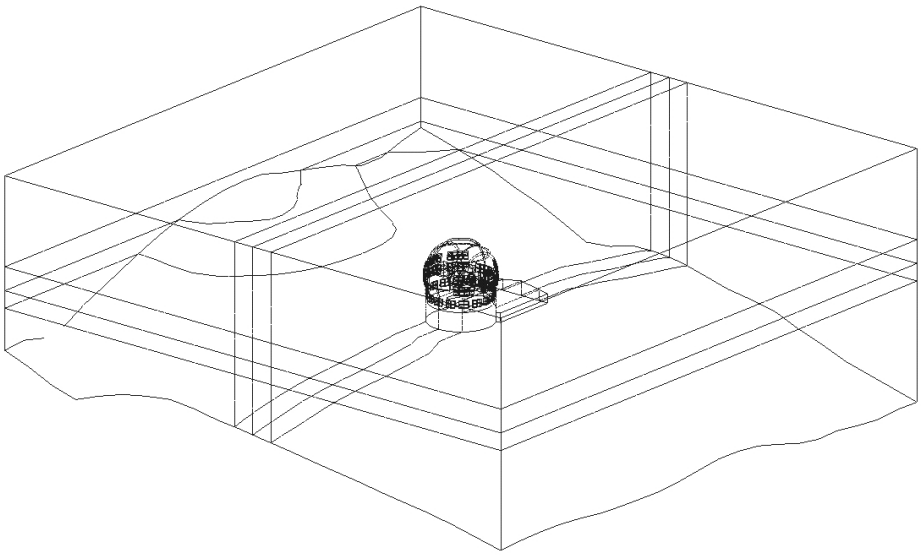

Figure 3: General view of the computational domain surrounding the telescope

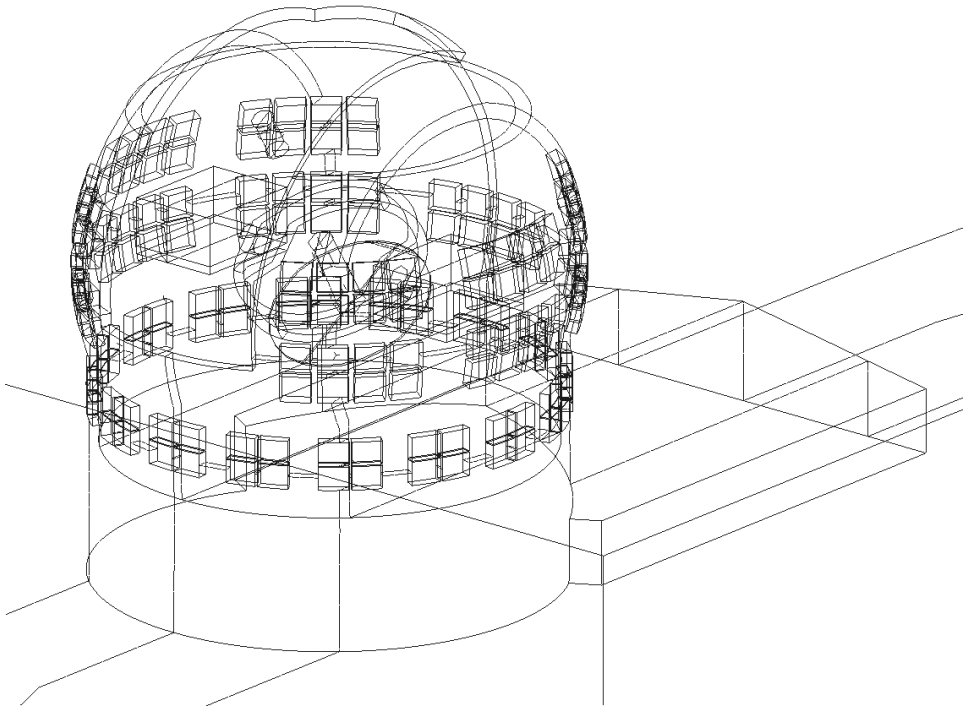

Figure 4: Sections on the telescope building

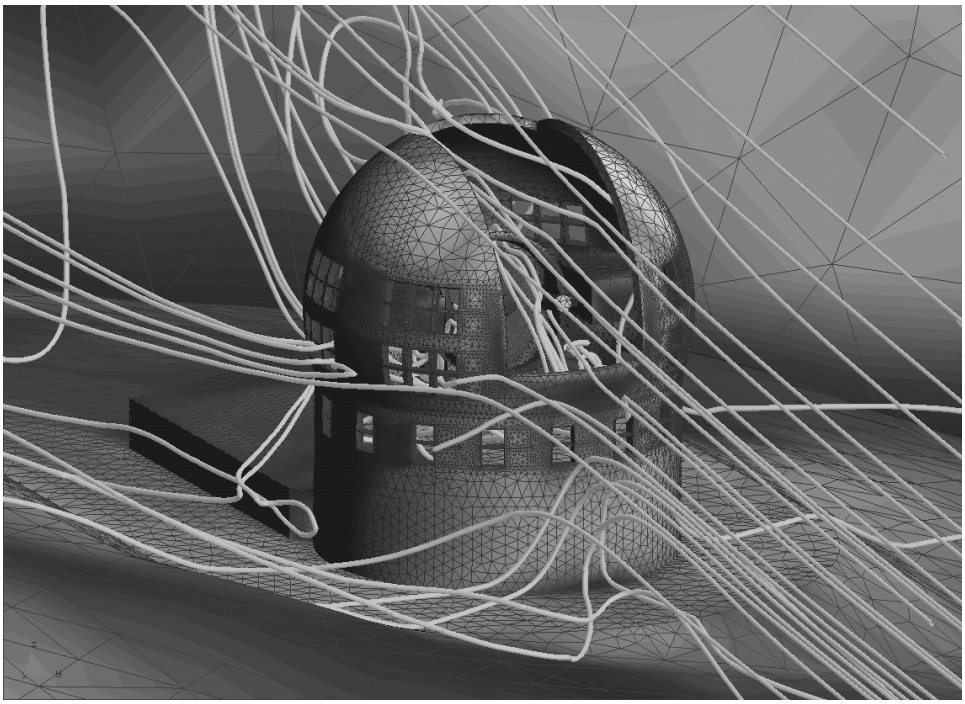

Figure 5: Surface mesh on the telescope building and some air particle paths

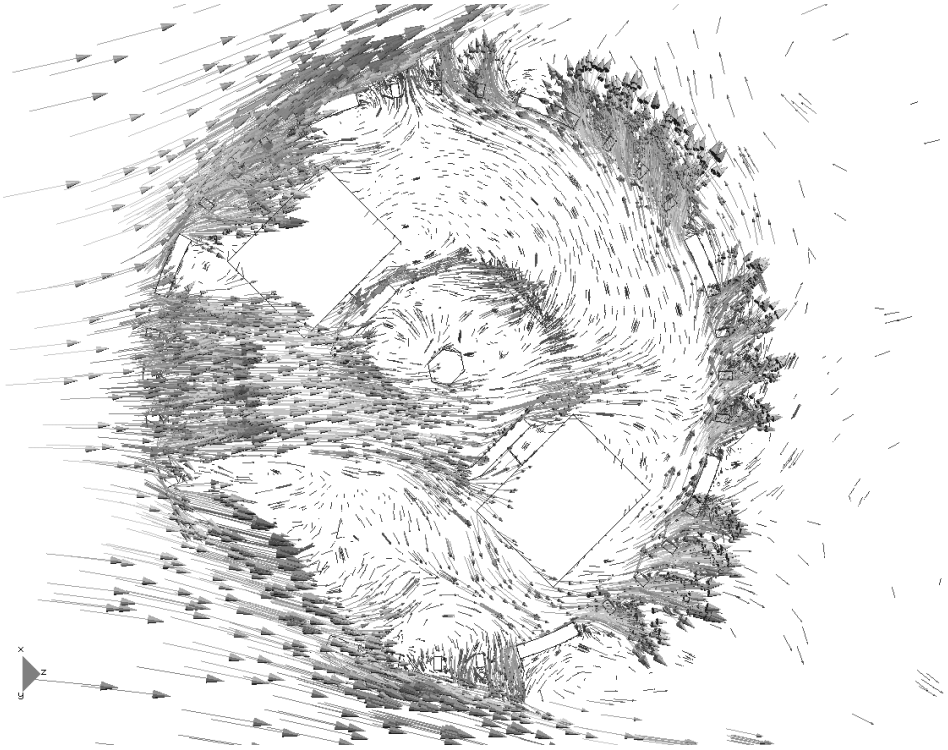

Figure 6: Example of velocity field on the horizontal mid section

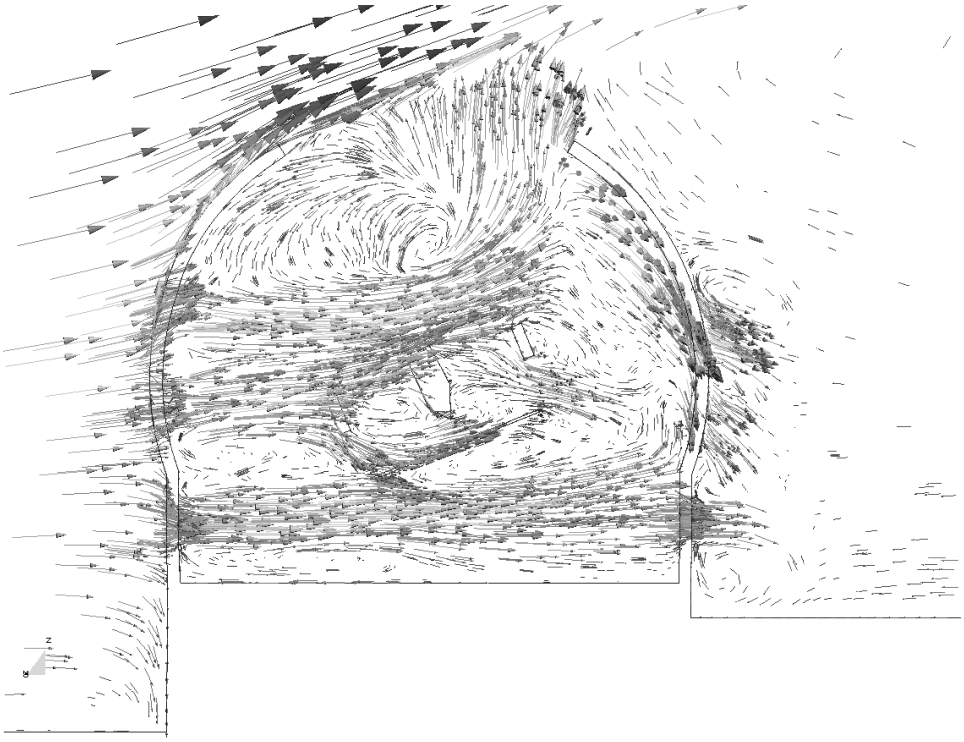

Figure 7: Example of velocity field on the vertical mid section

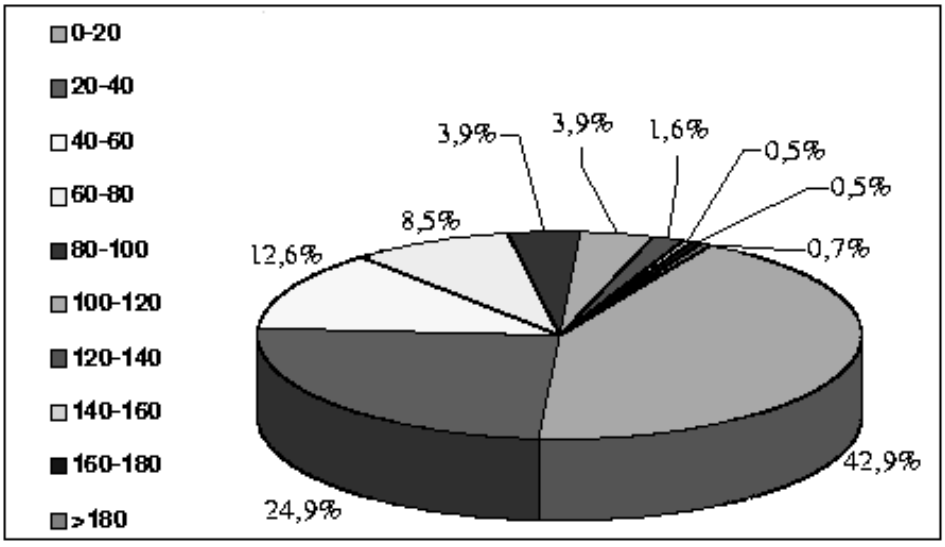

Figure 8: Example of distribution of average residence times

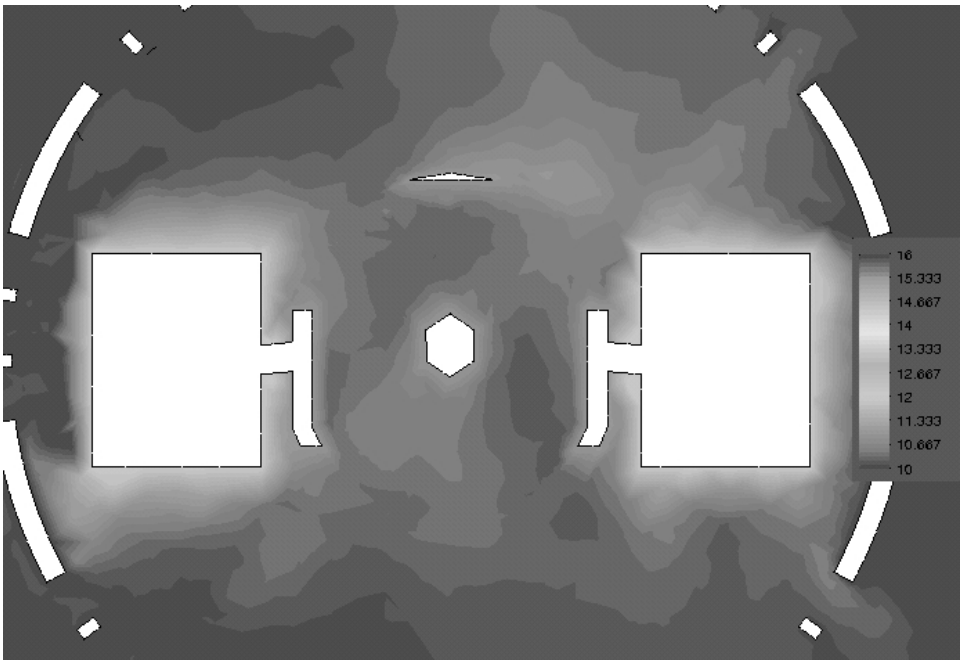

Figure 9: Example of temperature distribution on the horizontal mid section

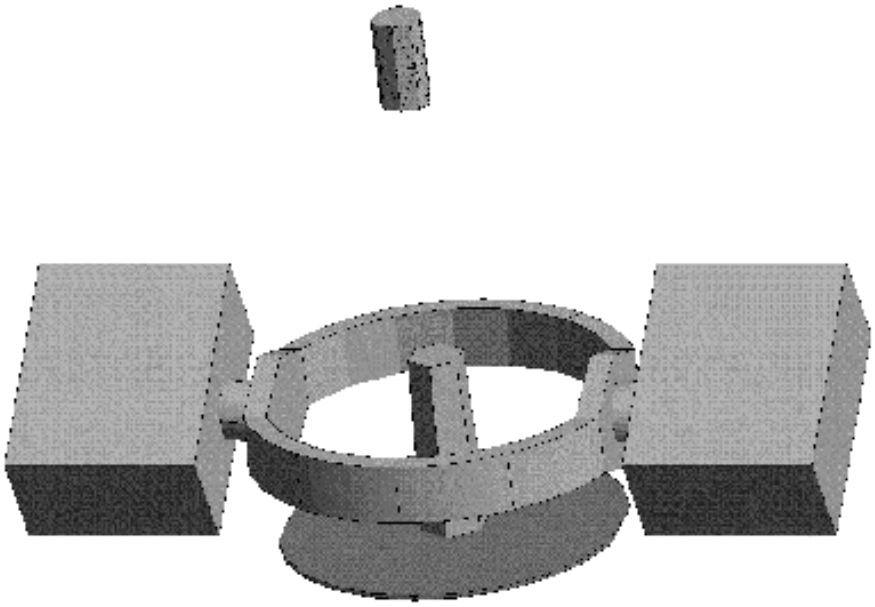

Figure 10: Instruments within the telescope on which forces have been computed

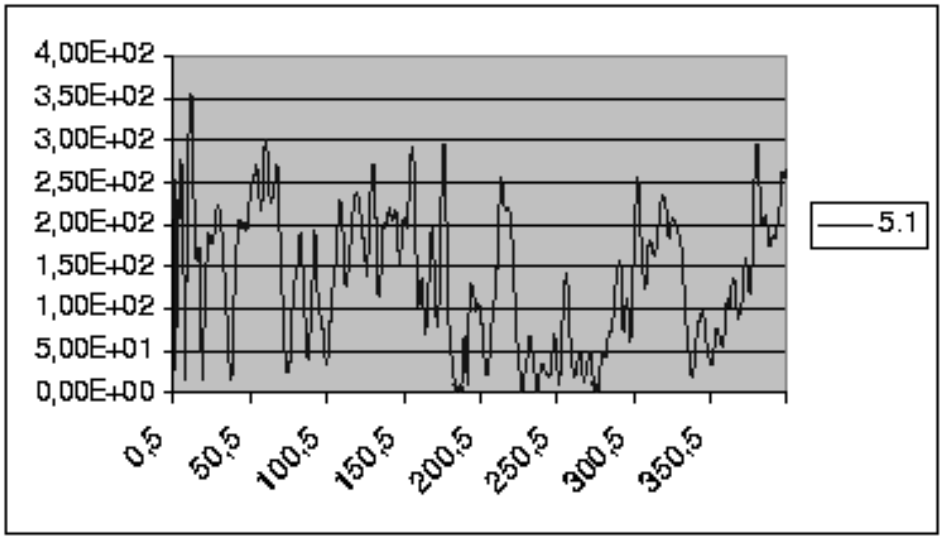

Figure 11: Total force (N) on the lower mirror computed for 10 m/s NW wind, over 400 s